# Geant4 simulation of the response of a veto detector with various beam energies for the measurement of charge-changing cross-section (CCCS) of 12C on a carbon target

By

**Saurav Mittal**

**(Admission No. 21MS0126)**

**Dissertation**

**SUBMITTED TO**

**INDIAN INSTITUTE OF TECHNOLOGY (INDIAN SCHOOL OF MINES), DHANBAD**

**For the award of the degree of**

**MASTER OF SCIENCE IN PHYSICS**

**MAY, 2023**

Form No: PG13

# INDIAN INSTITUTE OF TECHNOLOGY
# (INDIAN SCHOOL OF MINES) DHANBAD

CERTIFICATE FROM THE GUIDE

This is to certify that the Dissertation entitled **"Geant4 simulation of the response of a veto detector with various beam energies for the measurement of charge-changing cross-section (CCCS) of $^{12}$C on a carbon target"** being submitted to the Indian Institute of Technology (Indian School of Mines), Dhanbad, by Mr. **Saurav Mittal** , Admission No. **21MS0126** for the award of the Degree of **Master of Science** from IIT (ISM), Dhanbad, is a bonafide work carried out by him/her, in the **Department of Physics** , IIT (ISM), Dhanbad, under my/our supervision and guidance. The dissertation has fulfilled all the requirements as per the regulations of this Institute and, in my/our opinion, has reached the standard needed for submission. The results embodied in this dissertation have not been submitted to any other university or institute for the award of any degree or diploma.

Soumya Bagchi

_____

Signature of the Guide (s)

Name: **Prof. Soumya Bagchi**

Date: 12/05/2023

# DECLARATION

I hereby declare that the work which is being presented in this dissertation entitled **"Geant4 simulation of the response of a veto detector with various beam energies for the measurement of charge-changing cross-section (CCCS) of 12C on a carbon target"** in partial fulfillment of the requirements for the award of the degree of **Master of Science in Physics** is an authentic record of my own work carried out during the period from **January 2023** to **April 2023** under the supervision of **Prof. Soumya Bagchi**, Department of Physics**,** Indian Institute of Technology (ISM) Dhanbad, Jharkhand, India.

I acknowledge that I have read and understood the UGC (Promotion of Academic Integrity and Prevention of Plagiarism in Higher Educational Institutions) Regulations, 2018. These Regulations were published in the Indian Official Gazette on 31st July, 2018.

I confirm that this Dissertation has been checked for plagiarism using the online plagiarism checking software provided by the Institute. At the end of the Dissertation, a copy of the summary report demonstrating similarities in content and its potential source (if any) generated online using plagiarism checking software is enclosed. I herewith confirm that the Dissertation has less than 10% similarity according to the plagiarism checking software's report and meets the MoE/UGC Regulations as well as the Institute's rules for plagiarism.

I further declare that no portion of the dissertation or its data will be published without the Institute's or Guide's permission. I have not previously applied for any other degree or award using the topics and findings described in my dissertation.

Signature of the Student

Name of the Student : Saurav Mittal

Admission No. : 21ms0126

Department : Physics

# ACKNOWLEDGEMENT

I would like to express my heartiest gratitude to Prof. Soumya Bagchi for being an excellent supervisor to me. He have motivated me to give my best in this project and he has inspired me to pursue a research career. I would also want to extend my heartiest thank to the junior research fellow (JRF) Debodyuti Kar for discussions and helping me to come up with a solutions. Finally, I would like to express my heartfelt gratitude to my friends and my family for their unwavering support.

Saurav Mittal
Department of Physics
IIT(ISM), Dhanbad

# ABSTRACT

Nuclear size, defined as root-mean-square charge-distribution radii is an important nuclear quantity for studying nuclear structure and properties. The traditional method of electron scattering and isotopic shift have some limitations and can't be extended to calculating charge-distribution radius of unstable nucleus. Therefore charge-changing cross section is a versatile technique for calculating charge-distribution radius of unstable nucleus. During the experiment some beam particle never hits the target but are included in calculation of charge-changing cross section. To isolate such events and improve the charge-changing cross section, we have proposed a veto detector. In this work we are studying the response of veto detector for various beam energies on the charge-changing cross section.

# Contents

# List of Figures

# List of Tables

# Chapter 1: Introduction

## 1.1 Charge-distribution radius

Nuclear size, usually defined as root-mean-square charge-distribution radii is an important nuclear quantity to extract information about the nuclear structure, and properties of dense nuclear structures such as neutron stars [1]. Knowledge of nuclear shell structure can help us understand the abundance of element in universe [2]. Electron scattering has been a primary technique used for the measurement of charge-distribution radius however for short-lived nuclei such measurements are still not possible. The isotope shift technique is another technique that is used for the measurement of charge-distribution radius in the light neutron-rich nuclei. However, it is difficult to extend the technique to the drip line due to weak beam intensities [3].

Therefore the charge-changing cross section is a versatile tool to measure charge-distribution radius. It is nothing but the proton removal cross section [4].

## 1.2 Charge-changing cross section

When a beam with sufficient energy passes through a target, a proton may get knocked out due to interaction with the target. The loss of proton results in the change of atomic number. The cross section of this change in the atomic number is called charge-changing cross section

If a beam of $N_o$ particles passes through matter and out of these $N_{samez}$ particles pass uninteracted, then the charge-changing cross section relation is defined as [5]

$$N_{samez} = N_o e^{-\sigma_{cc} t} \tag{1.1}$$

Where $\sigma_{cc}$ is the charge-changing cross section and t is the target thickness in

gm/cm$^2$. Counting the number of incident particles and the number of particles emerging with the same atomic number after passing through the target (these are the uninteracted particle), the charge-changing cross section can be calculated as [6]

$$\sigma_{cc} = \frac{1}{t} ln \frac{N_o}{N_{sameZ}} \tag{1.2}$$

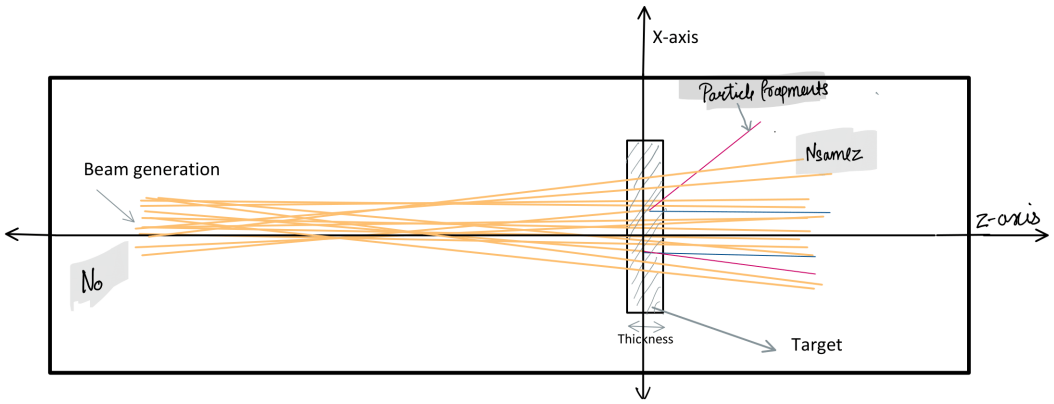


Figure 1.1: Charge-changing cross section measurement

There are chances that some nuclear reaction might occur in the non-target material (such as the detector window) while the beam propagates. This effect is accounted for by including the measurement without the target in the setup. The $\sigma_{cc}$ can be given as

$$\sigma_{cc} = \frac{1}{t} ln \frac{R_{w/o}}{R_w} \tag{1.3}$$

where $R_w$=$N_{sameZ}/N_o$ is the transmission ratio with target and $R_{w/o}$ is the transmission ratio without target.

## 1.3 Experimental Setup

The experimental setup consists of a particle ($^{12}$C,$^{16}$O) beam having certain energy. The beam is confined to move in a particular direction, say z-axis, and hitting a target. The target has thickness of a few gm/cm$^2$ in the z-axis and is made up of material such as carbon. When the beam has sufficient energy and it hits the target, a proton may get knocked out due to interaction with the target. An ionization chamber is placed behind the target. We can calculate the charge-changing cross section by counting the number of incident particles $N_o$ and the number of particles that emerges with the same atomic number after passing through the target i.e. $N_{samez}$. $N_{samez}$ can be counted by studying the peak of uninteracted event in the energy loss histogram of ionization chamber.

The beam particle are projected with momentum in random direction. Controlling their direction is limited to some extend so there can be case where a incident beam never hits the target but still gets considered in calculation. We have developed veto detector to isolate such events from our calculation.

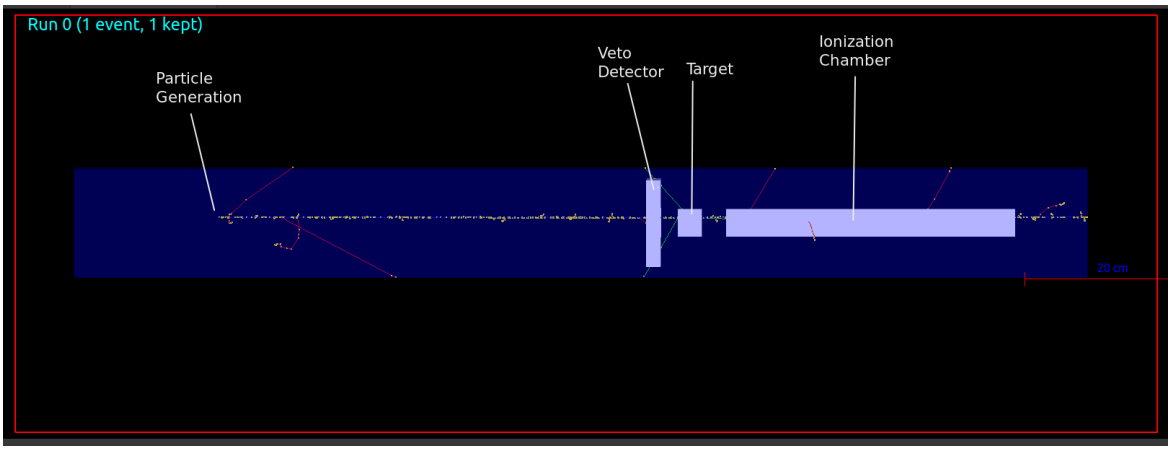


Figure 1.2: Schematic representation of experimental setup

## 1.4 Glauber model

From the charge-changing cross section we can get the charge-distribution radius by implementing it into the Glauber model. In glauber model take a standard optical limit approximation, [3]

$$\sigma_{cc} = \int\int 1 - |exp[i\xi(b)]|^2 db \tag{1.4}$$

$$i\xi(b) = \int\int_p\int\int_t \sum_i \rho^z_{p_p}(s)\rho^z_{T_i}(t)\Gamma_{pi}(b+s+t)dsdt \tag{1.5}$$

where $\rho_{T_i}$ (i=p,n) is the proton and density in the target $\rho_{p_p}$ is proton density of projectile. $\Gamma$ is the profile function.

Finite range glauber model we take a finite range for nuclear interaction. In the study we assume this range to be 0.39 fm. In Zero range glauber model we assume the range of interaction in zero and nucleons interact instantaneously. The Glauber model calculation for charge changing cross section are done using the C++ library i.e. Nurex library [7]. We have plotted these calculation for finite range and zero range Glauber model in figure below 1.3

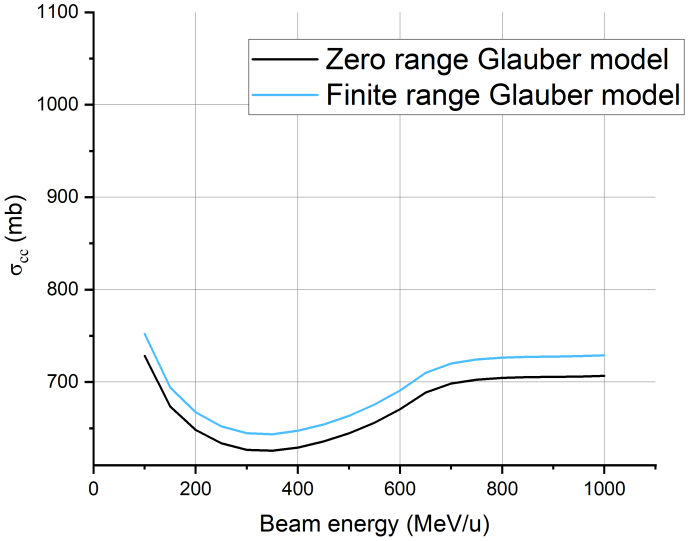


Figure 1.3: Glauber models theoretical prediction of charge changing cross section for different beam energies.

# Chapter 2: Setup for simulation

## 2.1 Softwares

### 2.1.1 Cern Root

Root is a software developed by CERN for data processing. It is written in C++ object-oriented language. Root feature an advanced graphical User interface which is ideal for analysis and C++ interpreter that is fast and effective [8].

### 2.1.2 Cern Geant4

**GE**omatary **AN**d **T**racking - Geant4 is a toolkit for creating simulations of the passage of particles through matter [9]. Geant4 can simulate detectors and radiation sources, and record physical quantities of interaction between projectile particles and the target material. Geant4 can be used for

- Create a model with shapes of different geometry and material.
- Locate points in the entire volume and navigate tracks inside the volume.
- Describe the physics of interactions of particles and the creation of secondary particles.
- Record selective information for various physical quantities.
- Visualize the setup and particle track.

## 2.2 Setup geometry

The simulation world is a long cuboid space filled with air. From one end of the world volume particle are projected toward the other end with a certain energy. At

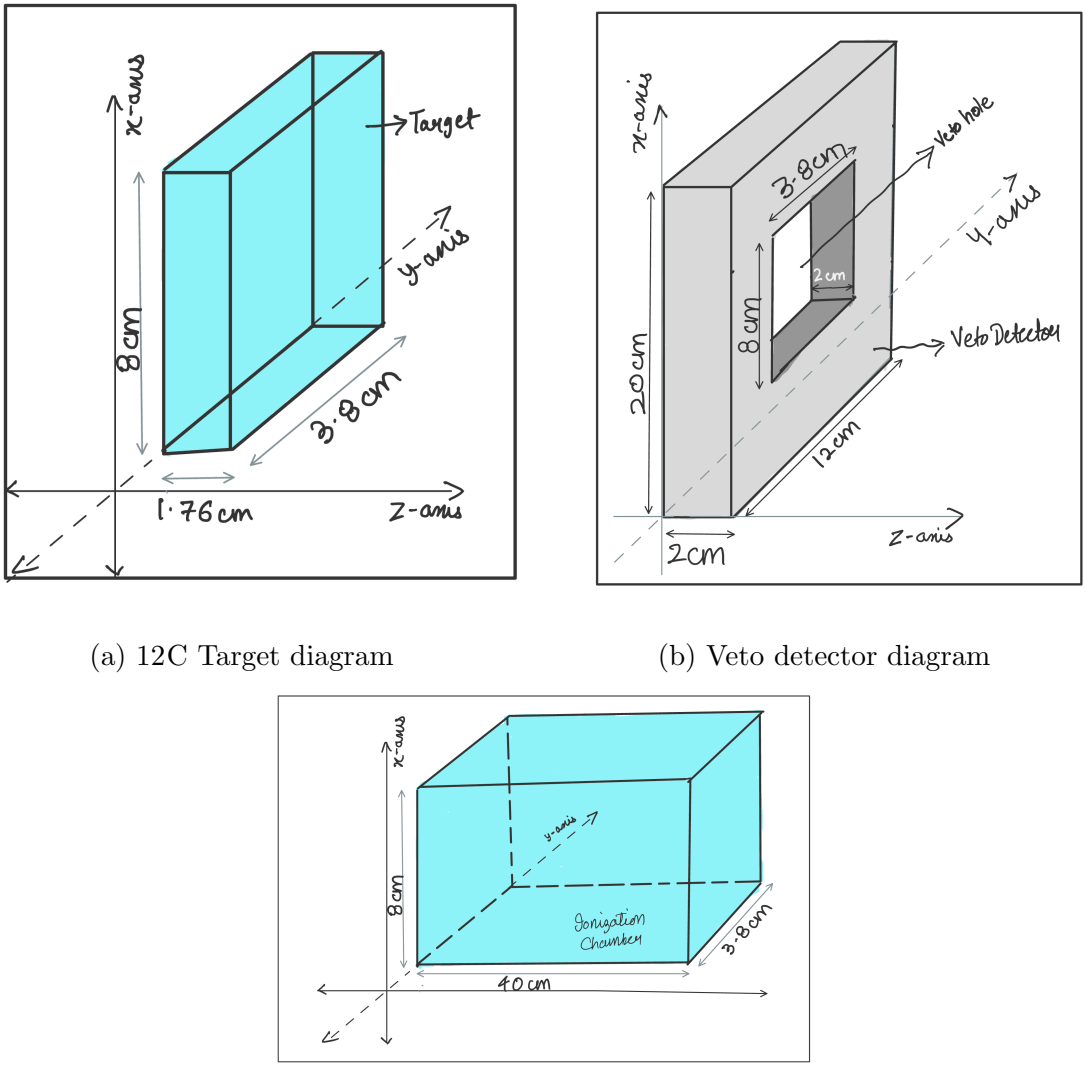


(a) 12C Target diagram

(b) Veto detector diagram

(c) Ionization chamber diagram

Figure 2.1: Schematic representation of various object used in simulation.

the other end, there is three geometry Veto Detector, Target, and Ionization chamber placed one after another.

Target also has a rectangular cross-section as shown in figure 2.1a. Targets of varying thickness are used for simulation such as 4 gm/cm$^2$. It is made up of carbon

($^{12}$C) with a density of 2.267 gm/cm$^3$. Veto Detector has a rectangular cross-section and thickness of 2 cm. It has a rectangular hole in the middle with the dimensions of target as shown in figure 2.1b. The veto detector is made of naphthalene with a density of 1.145 gm/cm$^3$.Ionization Chamber has a rectangular cross-section and thickness of 40cm as shown in figure 2.1c. The ionization chamber is filled with tetrafluoromethane ($CF_4$) with the density of gas 3.72 $\times$ $10^{-3} gm/cm^3$.

## 2.3 Particle beam

The $^{12}$C particle beam is generated with certain energy and momentum. The point of generation of momentum is randomized in the xy plane. The particles are projected along Z-axis with random angles ranging between -37.5 mrad to 37.5 mrad along X-axis and Y-axis. Particles having energy of 100 MeV/u, 200MeV/u, 300 MeV/u, 600 MeV/u, and 1000 MeV/u are studied in this work.

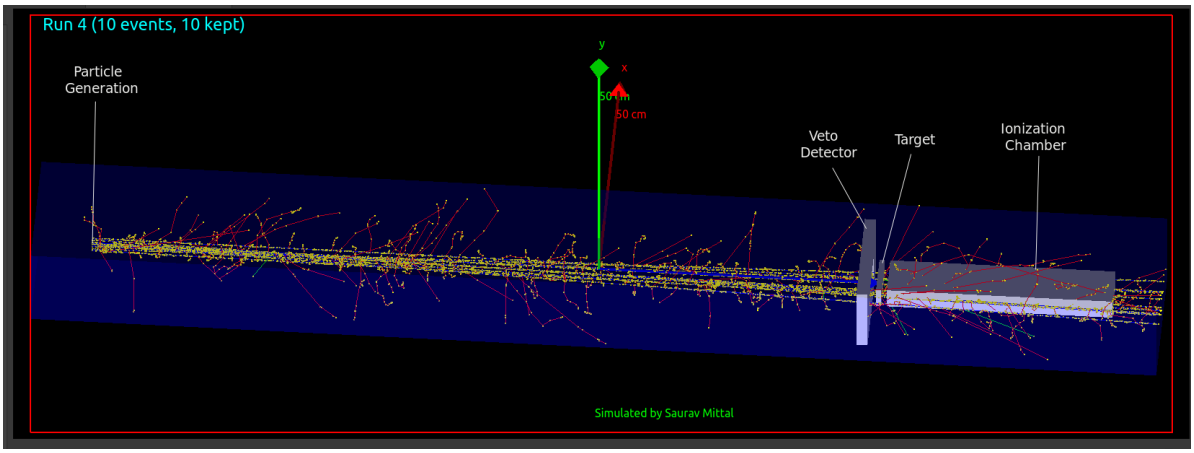


Figure 2.2: Particle beam generation

# Chapter 3: Methodology

The simulation is made to relate closely to real particle generation. The point of generation of the beam is randomized in the xy plane over a range of values. The momentum of the beam particle is along the z-axis with small randomized angles along X and Y-axis. Not all projectile particles are able to hit the target as the beam is generated from a large distance, and in some cases, it gets off track and misses the target. We design a veto detector to isolate these events from our calculation.

The veto detector is designed in such a way that there is a hole with the same aerial dimensions as target. The veto detector is placed in front of the target in such a way that for an event in which a beam goes off-track, it will hit the veto detector as shown in fig 3.1b. For the rest of the events, the beam will pass through the hole in the veto detector and hit the target as shown in fig 3.1b.

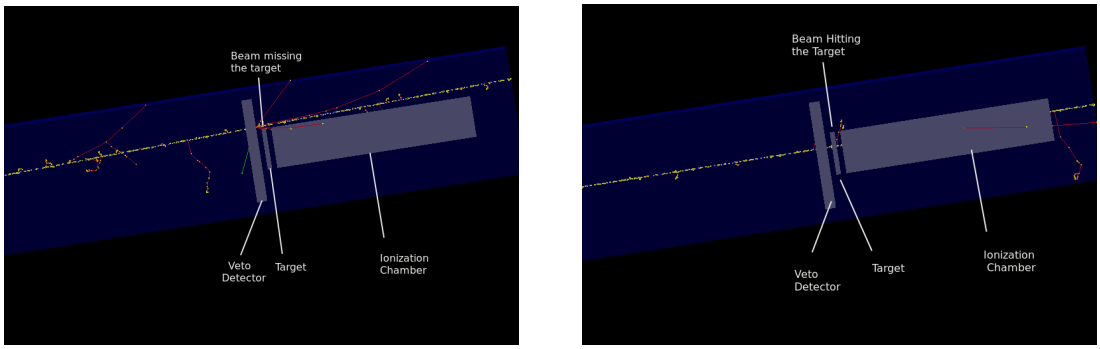


(a) Event where the beam hits Veto Detector (b) Event where the beam hits target

Figure 3.1: Schematic representation of different events where the beam hits the target or the veto detector

## 3.1 Energy deposition in veto detector

As ionization radiation passes through matter it transfers some of its energy to matter atoms by knocking out its electrons or taking the atoms to an excited state. Different categories of particles have different energy losses. The energy loss by the particle in the detector material is what is ultimately converted into the electronic signal pulse.

The energy loss per unit distance for heavy charged particles moving through matter at relativistic speeds is defined by the Bethe-Bloch formula [10]

$$-\frac{dE}{dX} \propto \frac{Z^2}{V^2} \tag{3.1}$$

where $z$ and $Z$ are the atomic number of the incident projectile and target(absorber) particle respectively, and V is the velocity of the projectile.

The energy loss of the veto detector is given by the distribution shown in fig 3.2a. The peak of the distribution with the highest number of counts denotes the energy loss inside the veto detector for that particular beam energy.

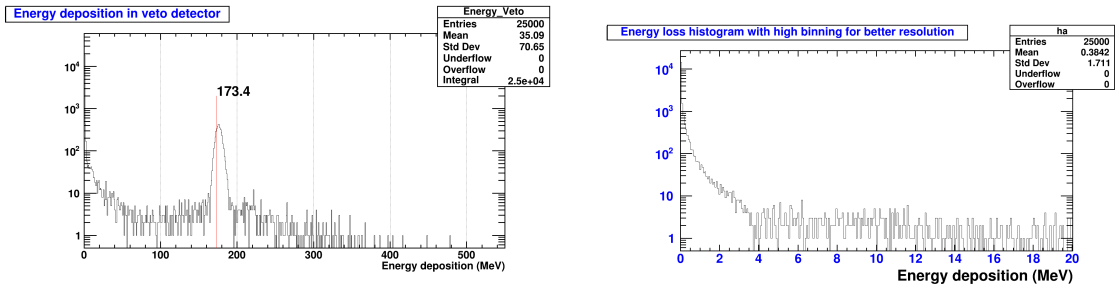


(a) Energy deposition distribution in veto detector

(b) X-axis range set to 0-20 Mev for energy loss histogram 3.2a

Figure 3.2: Energy deposition in veto detector

For the events that passed through the hole in the veto detector, there is no loss of energy. Such events are stacked at zero MeV energy with the peak tailing down to a few MeV energy on the energy loss histogram. This can be observed by setting the range of energy loss histogram to a few MeV energy as shown in fig 3.2b.

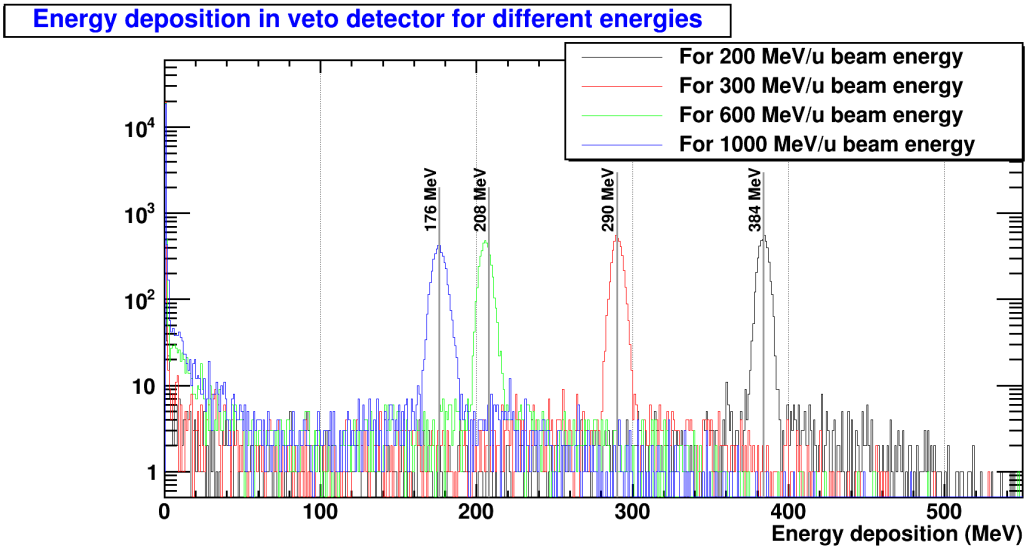


Figure 3.3: Energy loss histogram for different beam energies.

There are characteristic peaks for different beam energies. There is an inverse relation between beam energy and energy loss in the veto detector that can be seen in fig 3.3.

## 3.2 Back-scattered event

When the projectile particle hit the target there is a possibility of the particle breaking into fragments. These fragments can backscatter after the collision and travel back to hit the veto detector. The veto detector records the energy deposition of these fragments. We can observe these back-scattering events by comparing histograms with and without target as shown in fig 3.4a.

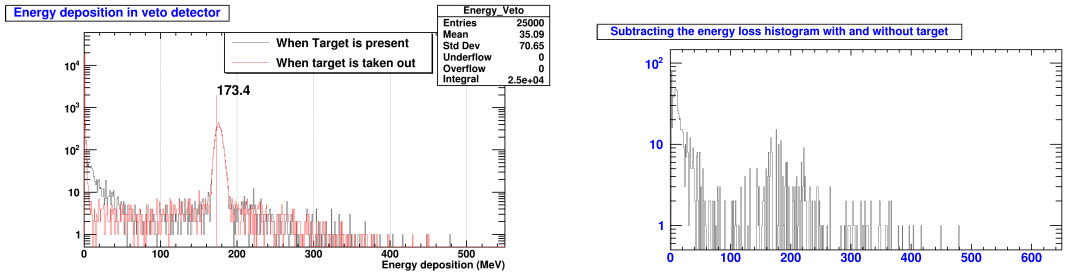


(a) Energy loss histogram with and without target

(b) Subtracting the energy loss histogram with and without target

Figure 3.4: Backscatteres Events

By subtracting these two energy loss histograms with similar binning and we can observe the back-scattering events that have happened due to the presence of the target as shown in fig 3.4b.

## 3.3 Threshold of veto energy

To calculate the charge-changing cross section we want to consider only those events in which the beam hits the target and does not backscatter. To isolate such events we put a threshold on energy loss in the veto detector. The energy threshold above which the events are rejected is called the veto cut. To determine the veto cut, the energy loss histogram of the veto detector with and without the target present is plotted together. By plotting the two histograms together with high binning we can visually identify the veto cut. The events that passed through the veto hole, are stacked at zero MeV energy with the peak tailing down to a few MeV energy on the energy loss histogram. The veto cut is somewhere near this tailed-down region.

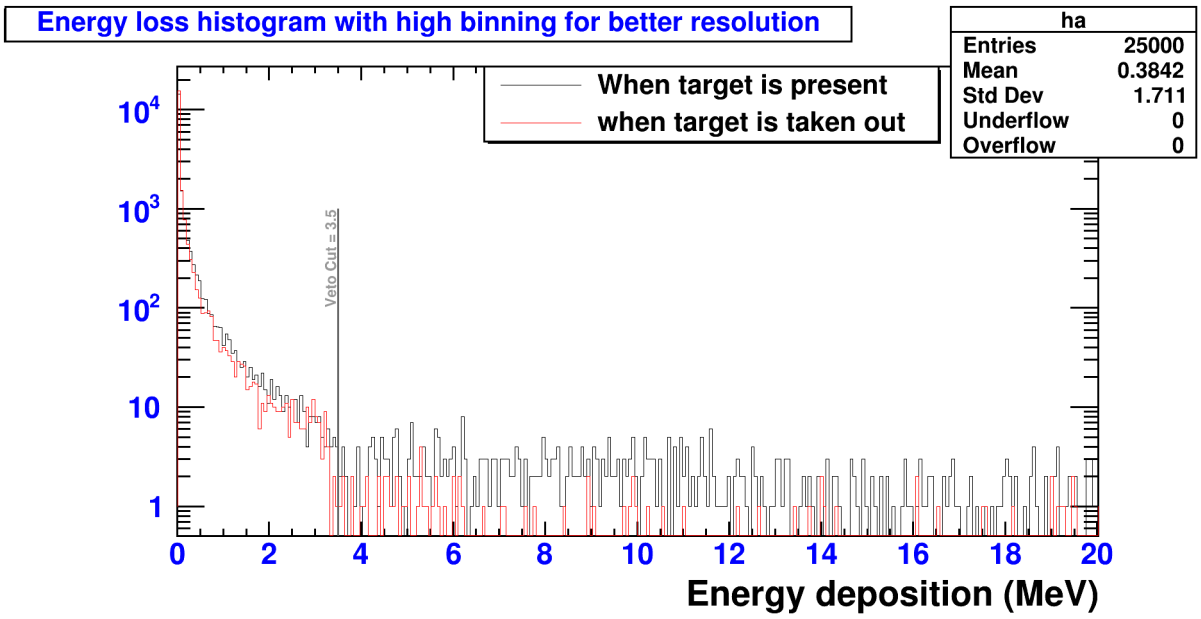


Figure 3.5: Zoomed-in histogram of Fig.(3.4a) with higher binning

For calculating the charge-changing cross-section we want the number of events that are within the veto cut i.e. $N_o$. We can calculate $N_o$ by summing all the events that happened within the range of zero MeV on the lower side and veto cut on the upper side.

## 3.4 Selection of target thickness

When the projectile particle propagates through the target, a proton can get knocked out of its nucleus, and its atomic number changes. We want to calculate the cross section of this change in the atomic number of the projectile nucleus. We need to carefully select the thickness of the target considering the beam energy. Because if the target is too thin we won't see a lot of nuclear reaction. On the other hand, if the target is too thick then the entire beam will get absorbed by the target.

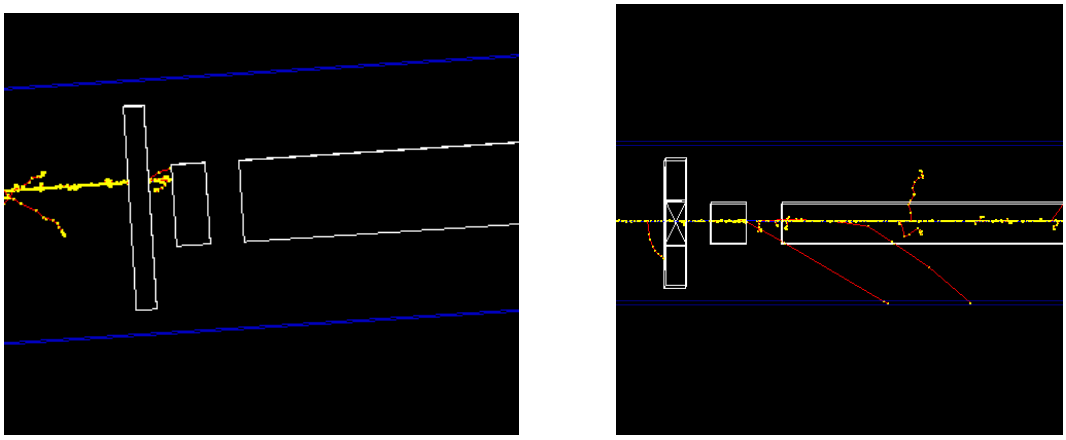

(a) Target is too Thick (b) Target is adequately thick

Figure 3.6: Selection of target thickness

The target thickness can be calculated using the formula

$$t = d \times \frac{N_a}{M_c} \tag{3.2}$$

Where d is the thickness of target in $g/cm^2$, $N_a$ is the Avogadro's number. $M_c$ is the mass of target and we are using a carbon target.

## 3.5 Energy response from the ionization chamber

As the projectile particle passes through the target, one or more protons can get knocked out of its nucleus. After passing through the target the projectile then enters the ionization chamber. Inside the ionization chamber, we record energy deposition for the particle for each event. The energy loss is directly proportional to the square of atomic number according to the Bethe-Bloch formula. So if the projectile has lost a proton there would be correspondingly less energy deposition inside the ionization chamber. We observe multiple peaks in the energy deposition histogram of the ionization chamber. The peak with the highest number of counts is the one where the particle passed through the target unreacted without losing any

proton. The next peak is for the events where a single proton is knocked out and so on.

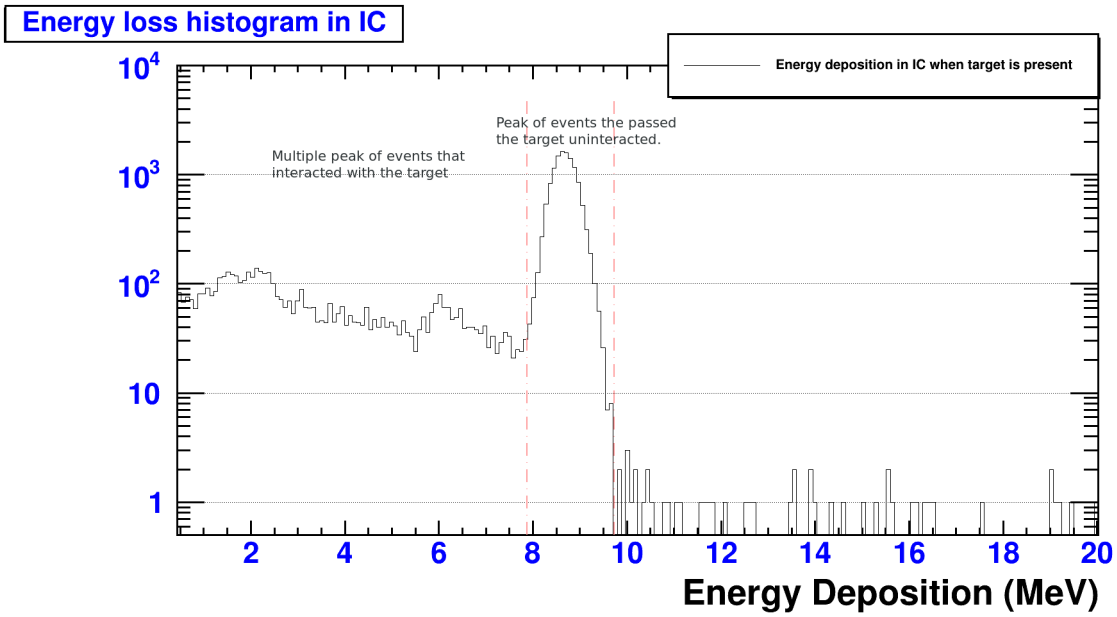


Figure 3.7: Different peaks in energy deposition histogram of IC

For calculating the charge-changing cross-section we want the number of events that passed through the target uninteracted i.e. $N_{samez}$. We fit a gaussian distribution over the first peak and calculate its mean ($e_o$) and standard ($\sigma_o$)deviation. We can then calculate $N_{samez}$ by summing all the events that happened in the range ($e_o - 3.5\sigma_o$) on the lower side and on the upper side we have tried to include everything as there is no proton addition.

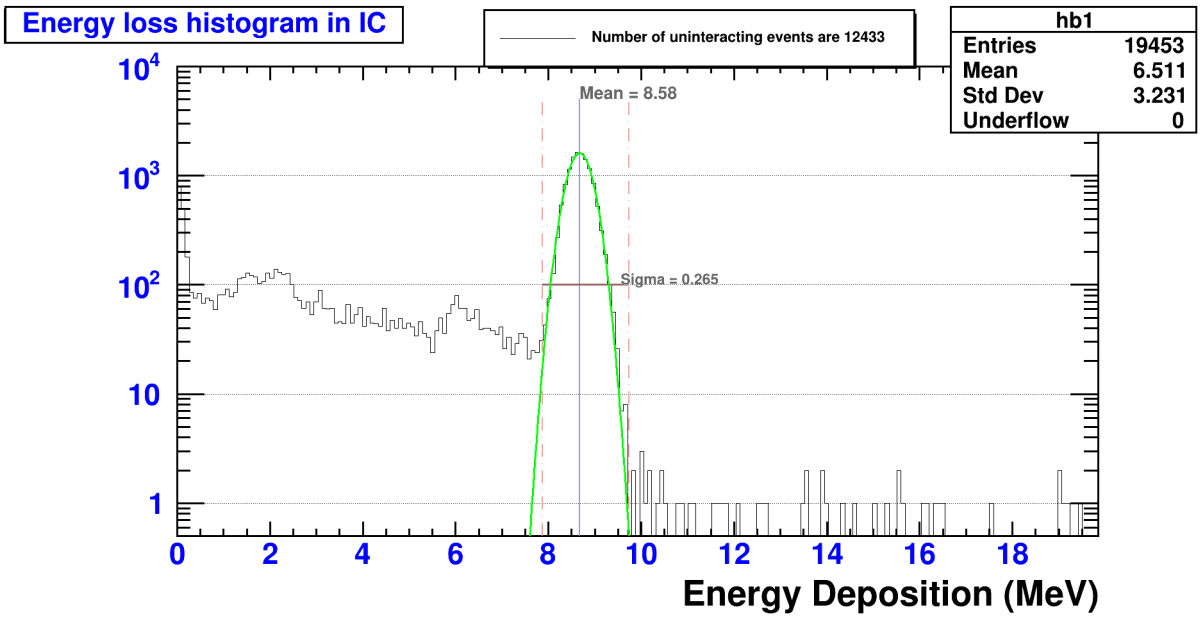


Figure 3.8: Number of uninteracting event when target is present

The energy deposition histogram when the target is taken out is shown in fig 3.9. Here we observe only a single peak since the target is taken out. We can count the number of uninteracted events i.e. $N_{samez}$ by repeating the method we used above. We want to add these to our calculation to account for any nuclear reactions that might occur in the non-target material while the beam propagates.

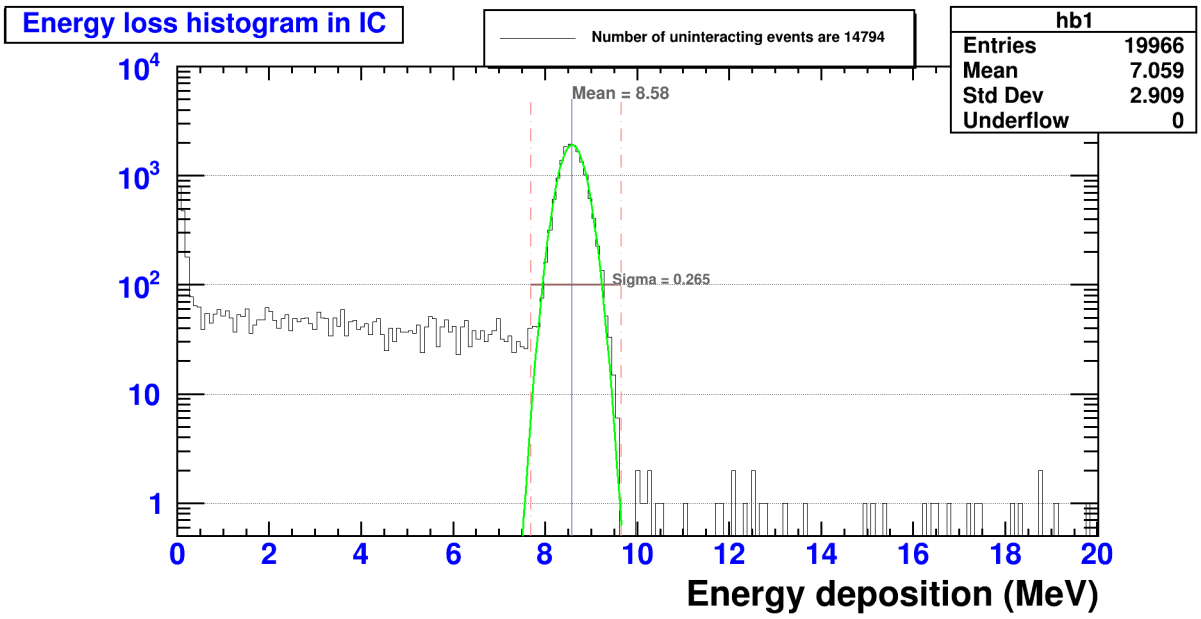


Figure 3.9: Number of uninteracting event when target isn't present

## 3.6 CCCS calculations

The transmission ratio is the ratio of the number of uninteracted events i.e. $N_{samez}$ and the number of events that are within the veto cut i.e. $N_o$. We have discussed how $N_o$ and $N_{samez}$ are calculated in the section 3.3 and 3.5 respectively.

$R_{in}$ is the transmission ratio with target present and $R_{out}$ is the transmission ration without target present. Once we know the transmission ratios the Charge-changing cross section can be obtained as

$$\sigma_{cc} = \frac{1}{t} ln \frac{R_{out}}{R_{in}} \tag{3.3}$$

Since this is a simulation we have control over the number of incident beams. When we are not taking veto cut into account all the incident beams are considered. Therefore when we are calculating charge-changing cross section without the veto cut $N_o$ becomes the total number of incident particles i.e. 25000 for this study.

After obtaining the cross section, the values will be compared with the Glauber model calculations

# Chapter 4: Results and conclusion

## 4.1 Energy deposition in veto detector

The energy deposition peak values are calculated by fitting a gaussian over the peak as discussed in Section 3.1. These values are then compared with the energy deposition value from WebAtima [11].

| | **Beam energy (MeV/u)** | **Peak energy deposition in veto detector (MeV)** | **Energy from webAtima (MeV)** | **Energy difference (MeV)** |
|---|---|---|---|---|
| 1 | 100 | 881.9 | 794.4 | 87.5 |
| 2 | 200 | 383.9 | 376.3 | 7.6 |
| 3 | 300 | 290.5 | 285.7 | 4.8 |
| 4 | 600 | 205.9 | 202.6 | 3.3 |
| 5 | 1000 | 175.7 | 173.4 | 2.3 |

Table 4.1: Energy deposition in veto detector

For 100 MeV/u beam energy, we can observe that the energy deposition value of veto detector varies a lot from the energy value from WebAtima. We observe this energy difference only at low energies. At low energy Fermi motion of nucleons also start playing a role in energy deposition. These corrections are not added in the Geant4 simulations.

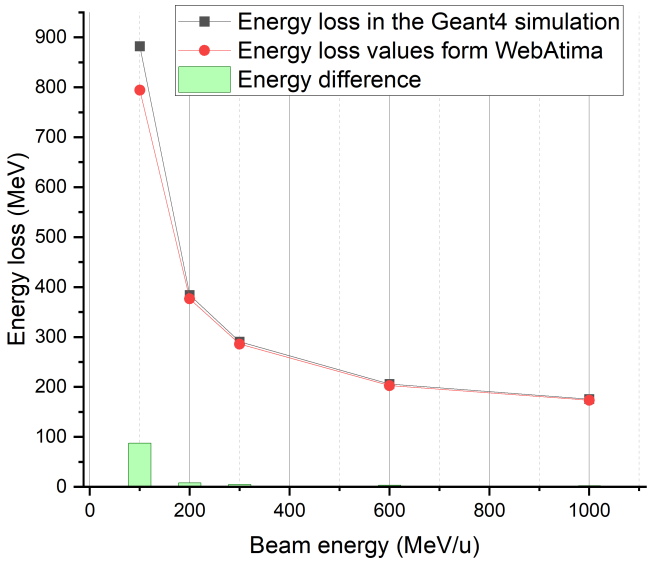


Figure 4.1: Comparision of energy deposition values from Geant4 simulation and WebAtima for veto detector

## 4.2 Veto cut for different beam energy

The veto cut for different beam energy is calculated using the method described in Section 3.3.

| | Beam energy (MeV/u) | Veto cut (MeV) |
|---|---|---|
| 1 | 100 | 0.65 |
| 2 | 200 | 1.1 |
| 3 | 300 | 1.4 |
| 4 | 600 | 1.8 |
| 5 | 1000 | 3.5 |

(a) Veto cut for different beam energies

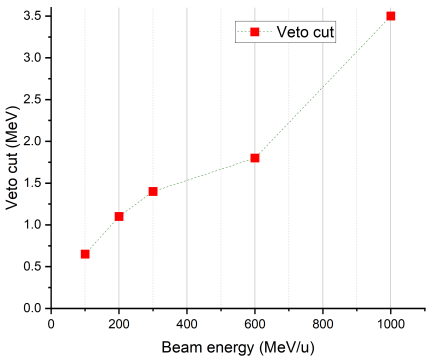


(b) Beam energy vs veto cut

Figure 4.2: Veto cut

## 4.3 CCCS Calculation

### 4.3.1 With veto cut

We considered beams of different energies (100 MeV/u, 200 MeV/u, 300 MeV/u, 600 MeV/u, and 1000 MeV/u) and targets of varying thickness (2 gm/cm$^2$, 3 gm/cm$^2$, and 4 gm/cm$^2$). We calculated the number of events that are within the veto cut i.e. $N_o$ and the number of events that passed through the target uninteracted i.e. $N_{samez}$ using the methods discussed in section 3.3 and 3.5 respectively. Charge-changing cross section (CCCS) is then calculated using the method discussed in section 3.6.

| | Beam energy ($MeV/u$) | Target thickness ($gm/cm^2$) | Target (with / without) | $N_{samez}$ | $N_o$ | $\sigma_{cc}$ (mb) |
|---|---|---|---|---|---|---|
| 1 | 100 | 2 | with | 13059 | 19870 | 1032 |
| | | | without | 14598 | 20039 | |
| 2 | 200 | 2 | with | 13567 | 19872 | 688 |
| | | | without | 14666 | 20056 | |
| 3 | 200 | 3 | with | 13030 | 19767 | 688 |
| | | | without | 14664 | 20056 | |
| 4 | 300 | 2 | with | 13629 | 19758 | 667 |
| | | | without | 14792 | 20063 | |
| 5 | 300 | 4 | with | 12666 | 19858 | 664 |
| | | | without | 14672 | 20134 | |
| 6 | 600 | 3 | with | 13057 | 19662 | 679 |
| | | | without | 14597 | 19844 | |
| 7 | 600 | 4 | with | 12575 | 19644 | 682 |
| | | | without | 14566 | 19844 | |
| 8 | 1000 | 4 | with | 12433 | 19453 | 737 |
| | | | without | 14794 | 19966 | |

Table 4.2: $\sigma_{cc}$ when veto cut is considered

### 4.3.2 Without veto cut

We want to calculate the charge-changing cross section without considering the veto cut. Since this is a simulation we have the control over total number of events. $N_o$ is the total number of events as discussed in section 3.6 and the $N_{samez}$ is calculated in the same way we did above. We then calculated the charge-changing cross section (CCCS) using the method discussed in section 3.6.

| | Beam energy ($MeV/u$) | Target thickness ($gm/cm2$) | Target (with / without) | $N_{samez}$ | $N_o$ | $\sigma_{cc}$ (mb) |
|---|---|---|---|---|---|---|
| 1 | 100 | 2 | with | 13064 | 25000 | 1114 |
| | | | without | 14600 | 25000 | |
| 2 | 200 | 2 | with | 13569 | 25000 | 784 |
| | | | without | 14673 | 25000 | |
| 3 | 200 | 3 | with | 13040 | 25000 | 783 |
| | | | without | 14671 | 25000 | |
| 4 | 300 | 2 | with | 13619 | 25000 | 742 |
| | | | without | 14665 | 25000 | |
| 5 | 300 | 4 | with | 12653 | 25000 | 738 |
| | | | without | 14666 | 25000 | |
| 6 | 600 | 3 | with | 13084 | 25000 | 733 |
| | | | without | 14610 | 25000 | |
| 7 | 600 | 4 | with | 12599 | 25000 | 733 |
| | | | without | 14596 | 25000 | |
| 8 | 1000 | 4 | with | 12458 | 25000 | 859 |
| | | | without | 14802 | 25000 | |

Table 4.3: $\sigma_{cc}$ when veto cut is not considered

## 4.4 Without veto detector in setup

| | **Beam Energy** ($MeV/u$) | **Target Thickness** ($gm/cm2$) | **Target (with / without)** | $N_{samez}$ | $N_o$ | $\sigma_{cc}$ **(mb)** |
|---|---|---|---|---|---|---|
| 1 | 100 | 2 | with Target | 13086 | 25000 | 1142 |
| | | | without Target | 14638 | 25000 | |
| 2 | 200 | 2 | with | 13608 | 25000 | 820 |
| | | | without | 14768 | 25000 | |
| 3 | 300 | 2 | with | 13655 | 25000 | 821 |
| | | | without | 14820 | 25000 | |
| 4 | 600 | 4 | with | 12680 | 25000 | 808 |
| | | | without | 14913 | 25000 | |
| 5 | 1000 | 4 | with | 12749 | 25000 | 739 |
| | | | without | 14787 | 25000 | |

Table 4.4: $\sigma_{cc}$ when veto detector is removed from simulations

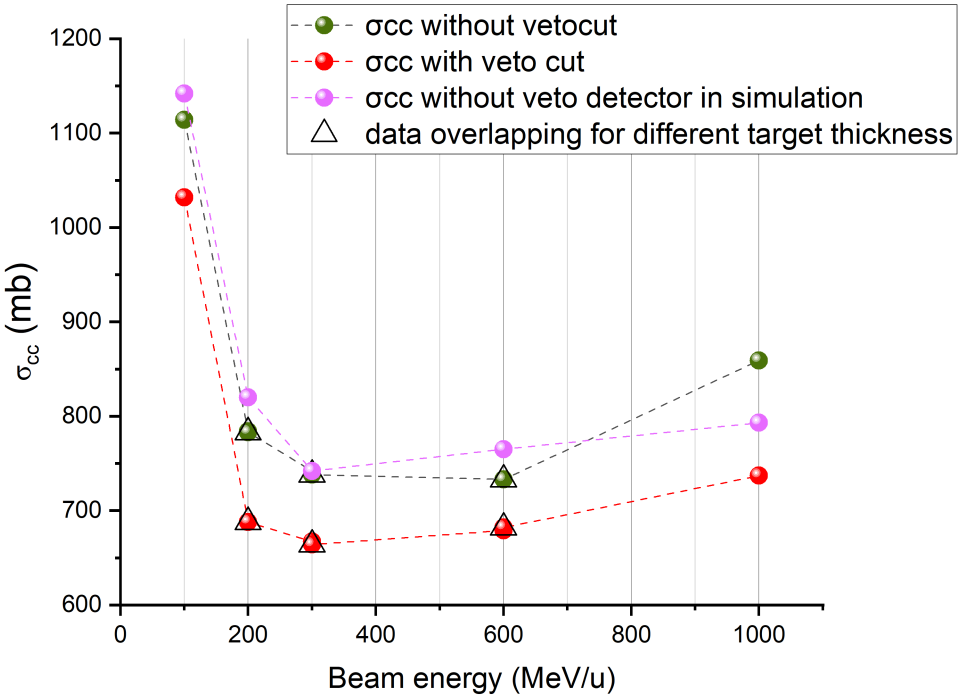


Figure 4.3: $\sigma_{cc}$ values for different condition on veto detector

We can conclude that the value of charge-changing cross section for a particular beam energy does not depend on target thickness. We can observe in the histogram that the CCCS overlaps for different thicknesses for 200 MeV/u, 300 MeV/u and 600 MeV/u beam energy.

## 4.5 Glauber model

The glauber model predicts theoretical values of charge-changing cross section. We compare these values with the results we obtained for the two case we have studied in the previous section.

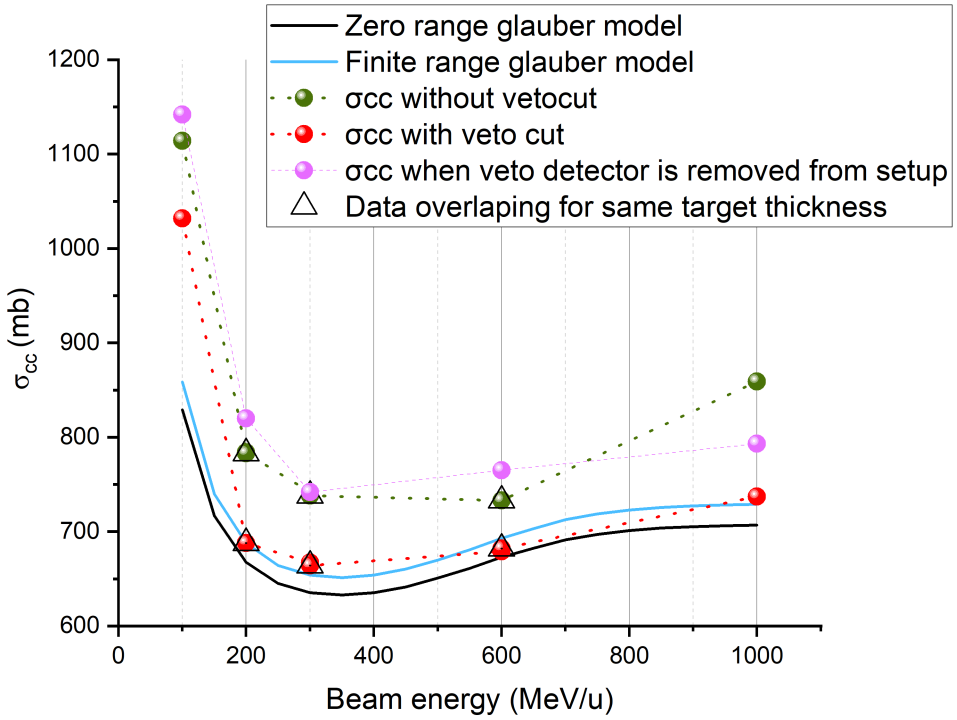


Figure 4.4: CCCS vs Beam Energy

From the above figure we can conclude that our results matches quite well for higher energy($<$ 100 MeV/u) with theoretical predictions of glauber model. With the presence of Veto cut, the CCCS values are further improved and almost matches with theoretical prediction of finite-range Glauber model.

# Chapter 5: Summary and conclusion

We have calculated the charge-changing cross section for a beam of particle hitting a target. We have compare these values with glauber model calculations and obtain charge-distribution radius. We have developed a veto detector and studied its response for different beam energies on charge-changing cross section measurement. We have calculated the charge-changing cross section value for the three different cases, without veto detector, with veto detector, without veto cut. We have then compared these values with the glauber model calculations. With the presence of veto detector, the charge-changing cross section values are improved and almost matches with finite range glauber model. We can conclude that by including veto detector in experimental setup we can significantly improve our calculations.

# References


[1] D. T. Tran et al. "Charge-changing cross-section measurements of $^{12--16}$C at around 45$A$ MeV and development of a Glauber model for incident energies 10$A$−−2100$A$ MeV". In: *Phys. Rev. C* 94 (6 Dec. 2016), p. 064604. DOI: 10.1103/PhysRevC.94.064604. URL: https://link.aps.org/doi/10.1103/PhysRevC.94.064604.

[2] S. Kaur et al. "Proton Distribution Radii of $^{16--24}$O: Signatures of New Shell Closures and Neutron Skin". In: *Phys. Rev. Lett.* 129 (14 Sept. 2022), p. 142502. DOI: 10.1103/PhysRevLett.129.142502. URL: https://link.aps.org/doi/10.1103/PhysRevLett.129.142502.

[3] A. Estradé et al. "Proton Radii of $^{12--17}$B Define a Thick Neutron Surface in $^{17}$B". In: *Phys. Rev. Lett.* 113 (13 Sept. 2014), p. 132501. DOI: 10.1103/PhysRevLett.113.132501. URL: https://link.aps.org/doi/10.1103/PhysRevLett.113.132501.

[4] R. Kanungo et al. "Proton Distribution Radii of $^{12--19}$C Illuminate Features of Neutron Halos". In: *Phys. Rev. Lett.* 117 (10 Sept. 2016), p. 102501. DOI: 10.1103/PhysRevLett.117.102501. URL: https://link.aps.org/doi/10.1103/PhysRevLett.117.102501.

[5] S. Bagchi et al. "Neutron skin and signature of the N = 14 shell gap found from measured proton radii of 1722N". In: *Physics Letters B* 790 (2019), pp. 251–256. ISSN: 0370-2693. DOI: https://doi.org/10.1016/j.physletb.2019.01.024. URL: https://www.sciencedirect.com/science/article/pii/S0370269319300401.

[6] Satbir Kaur. "DETERMINATION OF PROTON RADII OF NEUTRON-RICH OXYGEN ISOTOPES FROM CHARGE-CHANGING CROSS SECTION MEASUREMENTS". In: 2018.

[7] Isotopea. *Nurex - Glauber Model Calculator*. URL: https://www.isotopea.com/nurex/.

[8] Cern. *ROOT Data Analysis Framework*. URL: https://root.cern/.

[9] Cern. *GEANT4–a simulation toolkit*. URL: https://geant4.web.cern.ch/.

[10] Wikipedia contributors. *Bethe formula — Wikipedia, The Free Encyclopedia*. [Online; accessed 11-May-2023]. 2022. URL: https://en.wikipedia.org/w/index.php?title=Bethe_formula&oldid=1117291437.

[11] Isotopea. *WebAtima - Energy Loss Calculator*. URL: https://www.isotopea.com/webatima/.

# Chapter A: Appendix

The Simulation is done on Geant4 simulation [9]. And data is analysed with cern root [8].
The repository of this work is available at Github -
( https://github.com/Saurav131/VetoDetector)

# Saurav thesis

ORIGINALITY REPORT

| 7% | 5% | 4% | 1% |
|---|---|---|---|
| SIMILARITY INDEX | INTERNET SOURCES | PUBLICATIONS | STUDENT PAPERS |

PRIMARY SOURCES

| | | |
|---|---|---|
| 1 | dalspace.library.dal.ca<br>Internet Source | 2% |
| 2 | Zeitlin, C.. "Fragmentation cross sections of ^2^8Si at beam energies from 290A to 1200A MeV", Nuclear Physics, Section A, 20070301<br>Publication | 1% |
| 3 | slideplayer.com<br>Internet Source | 1% |
| 4 | es.slideshare.net<br>Internet Source | 1% |
| 5 | A. Estradé, R. Kanungo, W. Horiuchi, F. Ameil, J. Atkinson, Y. Ayyad, D. Cortina-Gil, I. Dillmann, A. Evdokimov, F. Farinon, H. Geissel, G. Guastalla, R. Janik, M. Kimura, R. Knöbel, J. Kurcewicz, Yu. A. Litvinov, M. Marta, M. Mostazo, I. Mukha, C. Nociforo, H. J. Ong, S. Pietri, A. Prochazka, C. Scheidenberger, B. Sitar, P. Strmen, Y. Suzuki, M. Takechi, J. Tanaka, I. Tanihata, S. Terashima, J. Vargas, H. Weick, J. S. Winfield. " Proton Radii of Define a | 1% |

Thick Neutron Surface in ", Physical Review Letters, 2014
Publication

---

6 "Handbook of Particle Detection and Imaging", Springer Science and Business Media LLC, 2021 <1%
Publication

---

7 D. T. Tran, H. J. Ong, T. T. Nguyen, I. Tanihata, N. Aoi, Y. Ayyad, P. Y. Chan, M. Fukuda, T. Hashimoto, T. H. Hoang, E. Ideguchi, A. Inoue, T. Kawabata, L. H. Khiem, W. P. Lin, K. Matsuta, M. Mihara, S. Momota, D. Nagae, N. D. Nguyen, D. Nishimura, A. Ozawa, P. P. Ren, H. Sakaguchi, J. Tanaka, M. Takechi, S. Terashima, R. Wada, T. Yamamoto. " Charge-changing cross-section measurements of at around MeV and development of a Glauber model for incident energies MeV ", Physical Review C, 2016 <1%
Publication

---

8 T. Yamaguchi, M. Fukuda, S. Fukuda, G. W. Fan et al. " Energy-dependent charge-changing cross sections and proton distribution of ", Physical Review C, 2010 <1%
Publication

---

9 www.iem.cfmac.csic.es <1%
Internet Source

---

Submitted to Indian School of Mines

| | | |
|---|---|---|
| 10 | Student Paper | <1% |
| 11 | ediss.uni-goettingen.de<br>Internet Source | <1% |
| 12 | Olmos Yáñez Bryan. "Simulación de la respuesta de una barra de plástico centelleador al flujo de muones cosmogénicos en ciudad universitaria", TESIUNAM, 2018<br>Publication | <1% |
| 13 | arxiv.org<br>Internet Source | <1% |

| | | | |
|---|---|---|---|
| Exclude quotes | On | Exclude matches | < 10 words |
| Exclude bibliography | On | | |